Biophysical Journal Volume 94 June 2008 4775–4782



# Attractive Forces between Cation Condensed DNA Double Helices

Brian A. Todd,* V. Adrian Parsegian,* Akira Shirahata,† T. J. Thomas,‡ and Donald C. Rau*

*Laboratory of Physical and Structural Biology, National Institute of Child Health and Human Development, National Institutes of Health, Bethesda, Maryland 20892-0924; †Department of Biochemistry and Cellular Physiology, Josai University, Saitama, Japan; and ‡Department of Medicine, University of Medicine and Dentistry of New Jersey-Robert Wood Johnson Medical School, Piscataway, New Jersey 08903

ABSTRACT By combining single-molecule magnetic tweezers and osmotic stress on DNA assemblies, we separate attractive and repulsive components of the total intermolecular interaction between multivalent cation condensed DNA. Based on measurements of several different cations, we identify two invariant properties of multivalent cation-mediated DNA interactions: repulsive forces decay exponentially with a 2.3 ± 0.1 Å characteristic decay length and the attractive component of the free energy is always 2.3 ± 0.2 times larger than the repulsive component of the free energy at force-balance equilibrium. These empirical constraints are not consistent with current theories that attribute DNA-DNA attractions to a correlated lattice of counterions. The empirical constraints are consistent with theories for Debye-Hückel interactions between helical line charges and with the order-parameter formalism for hydration forces. Each of these theories posits exponentially decaying attractions and, if we assume this form, our measurements indicate a cation-independent, 4.8 ± 0.5 Å characteristic decay length for intermolecular attractions between condensed DNA molecules.

## INTRODUCTION

Inside cells, viruses, and nanoparticles used for nonviral gene therapy, DNA is tightly packaged (''condensed'') by multivalent cations (1). Within these dense structures, DNA double helices remain separated by 7–12 Å of water, indicating a balance of long-range attractive and repulsive forces. Because the intermolecular interactions that stabilize these structures appear to be outside the scope of traditional theories for intermolecular forces, they have inspired development of new theories for more than 20 years. These include attractive electrostatic forces due to counterion correlations (2–5), screened Debye-Hückel interactions between helical molecules (6–8), and water-structuring or hydration forces (9,10). A lack of experimental measurements has prevented further development and discrimination among these alternate theories. Here, we combine single-molecule magnetic tweezers with osmotic stress on DNA assemblies. From these measurements, we distinguish attractive and repulsive components of the intermolecular interaction.

Attraction and repulsion are strikingly correlated. Despite structural and chemical differences among counterions and differences in the structure and energetics of the condensed DNA, we find that the attractive part of the free energy is always about twice the repulsive part of the free energy at force-balance equilibrium. Using this constraint and the experimentally observed 2.3 ± 0.1 Å exponentially decaying repulsive forces, we evaluate theories developed to describe forces between multivalent cation condensed DNA. Current theories for electrostatic counterion correlations (2–5) predict that the ratio of attractive to repulsive free energies should vary between 1.2 and 1.8 and are not consistent with our experimental observations. A ratio of attractive to repulsive free energy approximately equal to two was predicted for electrostatic interactions between helical molecules (6–8) and for hydration or water-structuring forces (9–11). If we assume the exponential form for attractive forces predicted by both of these theories, our measurements indicate a cation-independent 4.8 ± 0.5 Å characteristic decay length for attractions between multivalent cation condensed DNA. According to the interpretations of these theories, this characteristic decay length reflects either the 5.4 Å helical period of DNA (helical pitch/$2\pi$) (6–8) or the ~4 Å correlation length in liquid water (12).

## MATERIALS AND METHODS

### Reagents

Spermidine $[H_2N(CH_2)_3NH(CH_2)_4NH_2]$ trihydrochloride (Sigma-Aldrich, St. Louis, MO, No. S-2501), spermine $[H_2N(CH_2)_3NH(CH_2)_4NH(CH_2)_3NH_2]$ tetrahydrochloride (Fluka, Buchs, Switzerland, No. 85607), and $Co(NH_3)_6Cl_3$ (Sigma-Aldrich, No. H7891) were used as purchased, without further purification. The synthetic alkyl hexamine,1,21-diamino-4,9,13,18-tetraazaheneicosane $[H_2N(CH_2)_3NH(CH_2)_3NH(CH_2)_3NH(CH_2)_3NH(CH_2)_3NH_2]$ hexahydrochloride, was synthesized as previously described (13). We will abbreviate this compound as ''$sp^{6+}$'' to emphasize its homology with spermidine and spermine.

High molecular weight chicken blood DNA for osmotic stress measurements was prepared as previously described (14). Poly(ethylene glycol) (molecular weight 8000) was purchased from Fluka (Fluka Biochemika, microselect grade).

λ-DNA (Sigma-Aldrich, No. D3779) for magnetic tweezers measurements was biotinylated by first heating to 65°C to separate the cohesive ends and then incubated with Klenow polymerase (Sigma-Aldrich, No. D3779) in biotin-14-dATP (Invitrogen, Carlsbad, CA, No. 19524-016), biotin-14-dCTP (Invitrogen, No. 19518-018), dGTP, and TTP (Sigma-Aldrich, No. DNTP-100) for 1.5 h according to standard protocols (15). Streptavidin-coated latex beads (5 μm diameter) (Bang's Laboratories, Fishers, IN, No.

*Submitted December 7, 2007, and accepted for publication February 11, 2008.*

Address reprint requests to Brian A. Todd, E-mail: toddba@mail.nih.gov.

Editor: Jonathan B. Chaires.



0006-3495/08/06/4775/08 $2.00

doi: 10.1529/biophysj.107.127332

CP01N/7015) and 2.8 $\mu$m diameter streptavidin-coated paramagnetic beads (Dynal Biotech, Oslo, Norway, No. M270) were used as purchased.

All osmotic-stress and magnetic tweezers measurements were carried out in 10 mM Tris buffer (pH 7.4) at room temperature.

## Magnetic tweezers

The basic operation of our magnetic tweezers apparatus consists of a single $\lambda$-DNA molecule stretched between an immobile 5 $\mu$m bead and a 2.8 $\mu$m paramagnetic bead. The stretching force was controlled by varying the separation between the paramagnetic bead and a small neodymium magnet (Indigo Instruments, Waterloo, Ontario, Canada, No. 43534) positioned next to the microscope using a close-loop motorized micrometer (New Focus, San Jose, CA, No. 8310). The trajectory of the magnet was adjusted so that the magnetic force in the focal direction balanced the gravitational force on the magnetic particle. This kept the bead and, hence the net force, purely in the focal plane.

A 1.1 $\times$ 1.1 mm square cross-section glass capillary (Vitrocom, Mountain Lakes, NJ, No. 8280-050) was used for a flow cell. Similar procedures have coated the flow cell with streptavidin to immobilize one end of a biotinylated DNA (15). We found that coating caused the streptavidin-coated beads to adhere strongly to the surface. To circumvent this problem, we immersed a smaller 0.1 $\times$ 0.1 mm cross-section glass capillary (Vitrocom, No. 8505-050) in 1% biotinylated bovine serum albumin (Sigma-Aldrich, No. A8549), 10 mM Tris buffer for 45 min and inserted this into the flow cell. Five diameter streptavidin-coated beads (5 $\mu$m) were immobilized on the side of the smaller 0.1 $\times$ 0.1 mm glass capillary, circumventing problems with the beads adhering to the 1.1 $\times$ 1.1 mm flow cell. The edge of the 0.1 $\times$ 0.1 mm capillary can be seen as the vertical line abutting the 5 $\mu$m bead in Fig. 1.

A mix of $1 \times 10^6$ 5 $\mu$m beads and $1 \times 10^5$ 2.8 $\mu$m beads in 25 $\mu$L of 100 mM borate buffer (pH 8.0)/0.1% bovine serum albumin/0.01% $NaN_3$ was injected into a 50 mm length of the flow cell. The beads were allowed to sediment for ~5 min until they concentrated on the bottom of the flow cell. Biotinylated $\lambda$-DNA (1 fmol) in 25 $\mu$L of 100 mM borate buffer was then injected into the flow cell, and tubing attached. Pairs of beads attached by $\lambda$-DNA molecules were identified using optical tweezers to pull on the 5 $\mu$m latex particles and searching for ones with an attached 2.8 $\mu$m paramagnetic bead. When a set of tethered beads was identified, the optically trapped 5 $\mu$m particle was moved over to the 0.1 $\times$ 0.1 mm biotinylated bovine serum albumin-coated capillary, positioned ~10 $\mu$m from the bottom of the flow cell, and then pushed against the capillary wall until it adhered. The magnetic force was calibrated using the thermal fluctuations of the tethered paramagnetic bead (16). We confirmed that beads were tethered by a single DNA molecule by measuring the force-extension curve and verifying a persistence length of ~50 nm and a length of ~16 $\mu$m (17). Condensation forces were identified by stretching the DNA to >10 pN, filling the flow cell with a solution containing the condensing agents, and then decreasing the force at −0.1 pN/minute until condensation was observed. Bead positions in each frame were calculated from the centroid of intensity after background subtraction.

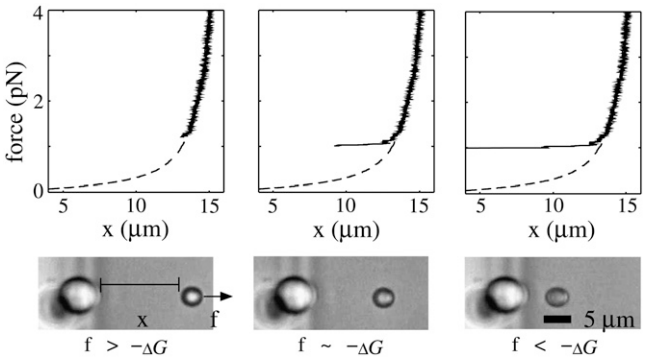


FIGURE 1 Measuring a condensation force in $Co(NH_3)_6Cl_3$. A single $\lambda$-DNA double helix is stretched between an immobilized bead (large bead on the *left*) and a bead susceptible to a magnetic force pulling to the right. Bathed in a solution containing the condensing agent, the DNA is initially stretched by a force, $f$, that is larger than the free energy of condensation, $\Delta G$. The force is gradually decreased and the distance between the beads, $x$, is monitored. Before condensation, the force-distance dependence is well characterized by the worm-like chain model (*dashed line*). At a critical force, $f \sim -\Delta G$, the bead-bead separation abruptly decreases. Within minutes, condensation of DNA reaches completion, bringing the magnetic bead nearly into contact with the fixed bead.

## Osmotic stress

The method for direct force measurement by osmotic stress has been described in detail by Parsegian et al. (18). In brief, condensed DNA arrays are equilibrated against a bathing polymer solution, typically polyethylene glycol (PEG) of known osmotic pressure that is excluded from the DNA phase. Water and salts are free to exchange between the PEG and condensed DNA phases. After equilibrium is achieved, the osmotic pressures in both the polymer and macromolecular phases are the same, as necessarily are the chemical potentials of all permeating species. The interhelical spacing can be determined as a function of the applied PEG stress by Bragg scattering of x-rays.

Spermidine, spermine, $sp^{6+}$, and $Co(NH_3)_6Cl_3$-precipitated DNA were prepared by slowly adding the multivalent ion in steps of ~0.2 mM to a 1 mg/ml (~3 mM DNA-phosphate) DNA solution in 10 mM TrisCl (pH 7.5) and mixing to a final nominal concentration of ~2 mM. Condensed DNA samples for the diamine putrescine were prepared by ethanol precipitating DNA from NaAcetate solutions. DNA pellets (~0.2–0.3 mg) were equilibrated against ~1 ml PEG solutions containing varying concentrations of the condensing ions in 10 mM TrisCl (pH 7.5) at room temperature for ~2 weeks with two changes of PEG solution and with occasional mixing. Osmotic pressures of the PEG solutions were measured directly using a Vapro Vapor Pressure Osmometer (model 5520, Wescor, Logan, UT). The x-ray scattering apparatus and data reduction are described in Hultgren and Rau (19).

# RESULTS

## Magnetic tweezers, $\Delta G$

The total free energy of DNA condensation per unit length can be measured by observing condensation of stretched single-molecules of DNA (20–22). In the presence of a sufficient concentration of multivalent cations, the ion-mediated condensation forces between helices oppose the magnetic force acting to extend the molecule. The energy balance between the favorable (negative) free energy of condensation and the work required to pull the magnetic bead against the magnetic force defines a phase transition (20–22). Under quasi-static equilibrium conditions (22), the collapse transition occurs when the total free energy is just less than zero, i.e., when the applied force is equal to the condensation free energy per unit length. An example of this measurement is shown in Fig. 1. The condensation free energy per unit length is determined simply as the force at which DNA transitions from extended to condensed (''condensation force''). Here, we combine measurements of the condensation forces for a hexavalent spermidine analog, $sp^{6+}$, with previous mea-

surements on cobalt hexammine, spermidine, and spermine (22).

As shown in Fig. 2, the condensation force depends strongly on multivalent ion concentration, $C$. Each multivalent cation exhibited a similar trend, rising from zero force at low concentration, reaching a maximum at intermediate concentration, and tending back toward 0 at high concentration. This behavior was previously observed for spermidine, spermine, cobalt hexammine, and protamine (22–24). The concentration dependence indicates, via a Gibbs-Duhem relationship, a difference in the number of bound multivalent cations between the extended and condensed phases (22). This contribution is proportional to $df/d\ln C$ and vanishes at the concentration where the condensing force is maximal. This condition was previously interpreted by Zhang and Shklovskii as the concentration where the extended DNA is, like the condensed DNA phase, electroneutral (25). Alternatively, the maximum condensation force could indicate the concentration where the energy gained by release of lower valent cation species balances the energy required to adsorb multivalent cations (22,26,27). In either case, the free energy measured at this concentration can be interpreted, in the absence of ion binding effects, as the free energy gain for bringing two helices with the appropriate number of adsorbed counterions for the condensed state from very far apart down to the equilibrium spacing, $\Delta G$. We extract $\Delta G$ for each ion by fitting a four-knot cubic spline (*lines* in Fig. 2) and extracting the peak value of the best-fit line. Table 1 lists $\Delta G$ in units of thermal energy per basepair for cobalt hexammine, spermidine, spermine, and a hexavalent spermidine analog, $sp^{6+}$ (12.3 pN = 1 $k_bT$/bp, with 3.4 Å for the basepair rise).

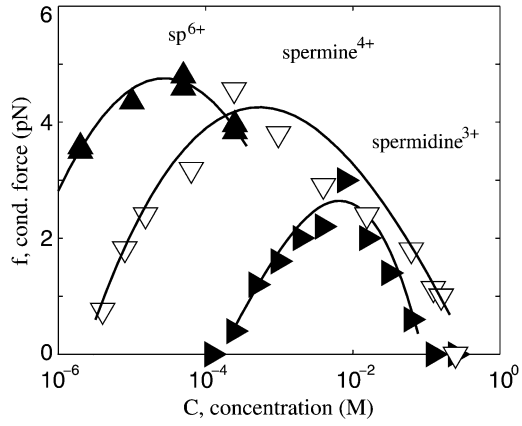


FIGURE 2 Concentration dependence of the condensation force for a hexavalent spermidine analog, $sp^{6+}$ (▲) and for the previously measured spermidine (►) and spermine (▽) (22). For each cation, the condensing force rises from 0 at low concentration, reaches a peak at intermediate concentration, and then decreases at high concentration. We fit each curve to a four-knot cubic spline (*lines*) and extracted $\Delta G$ from the peak value of the best-fit line. At the peak, the free energy is insensitive to condensing ion concentration and can be interpreted without the complicating energetic contributions for ion binding. Data for $Co(NH_3)_6Cl_3$ showed a similar inverted ''U'' shape (22) and a peak value was similarly extracted.

**TABLE 1 Combining osmotic stress and magnetic tweezers measurements**

| | $D_{eq}$, Å | $\Delta G$, $k_bT$/bp | $\Delta G_{rep}$, $k_bT$/bp | $\Delta G_{att}/\Delta G_{rep}$ |
|---|---|---|---|---|
| $Co(NH_3)_6Cl_3$ | 27.75 ± 0.1 | −0.21 ± 0.02 | 0.17 ± 0.01 | 2.2 ± 0.2 |
| Spermidine | 29.7 ± 0.1 | −0.20 ± 0.02 | 0.13 ± 0.02 | 2.5 ± 0.3 |
| Spermine | 28.15 ± 0.1 | −0.33 ± 0.03 | 0.29 ± 0.03 | 2.1 ± 0.2 |
| $sp^{6+}$ | 27.65 ± 0.1 | −0.38 ± 0.04 | 0.39 ± 0.07 | 2.0 ± 0.2 |

For each condensing ion, the net free energy, $\Delta G$, measured by magnetic tweezers and the repulsive component of the free energy, $\Delta G_{rep}$, measured by osmotic stress, are similar in magnitude. Subtracting the repulsive component from the total gives an attractive free energy that is about twice the repulsive free energy.

## Osmotic stress, $\Delta G_{rep}$

The repulsive contribution to the total condensation free energy measured by magnetic tweezers can be calculated from osmotic stress force curves (18). In osmotic stress, an ordered array of condensed DNA helices is equilibrated against a salt solution also containing a large sterically excluded polymer. The osmotic pressure exerted by the excluded polymer on the DNA phase acts to compact the DNA helices until the intermolecular pressure between the helices balances the solution osmotic pressure. A plot of the polymer osmotic pressure, $\Pi$, versus the intermolecular spacing between DNA helices measured by x-ray scattering, $D$, furnishes the intermolecular pressure-distance relationship for DNA under a particular set of solution conditions.

For DNA that is spontaneously condensed by multivalent cations (Fig. 3: $spermidine^{3+}$, *right triangles*; $spermine^{4+}$, *down open triangles*; a +6 charged alkyl hexamine, $sp^{6+}$, *up solid triangles*; $Co(NH_3)_6^{3+}$, *solid circles*), increasing osmotic pressure compacts DNA past its equilibrium spacing (indicated by *arrows*) to progressively smaller interhelical spacings. Concomitantly, the measured pressures shift from an equilibrium balance of attractions and repulsions to increasing dominance by the shorter-range repulsions. This allows the repulsive component of the total interaction to be isolated from the high pressure limit of the osmotic stress force curve. This can then be compared with the condensation free energy measured by magnetic tweezers by integrating the repulsive intermolecular pressure up to the equilibrium interhelical spacing to obtain a repulsive free energy, $\Delta G_{rep}$.

Within the experimentally accessible range of osmotic pressures, isolating the shorter-range repulsions from the measured total pressure is nontrivial. In the past, we have assumed that the curves reached a limiting exponential form at the highest pressures (or equivalently, smallest spacings) and extracted 1.4–1.6 Å decay lengths from high-pressure data (10). However, the curves had not reached a limiting behavior, so these values should be considered lower bounds. Fitting the same data to a biexponential form appropriate for either hydration forces or Debye-Hückel electrostatics gave a larger, 2.25 Å decay length for the repulsive component (10). We have fit each curve in Fig. 3 similarly, using an arbitrary

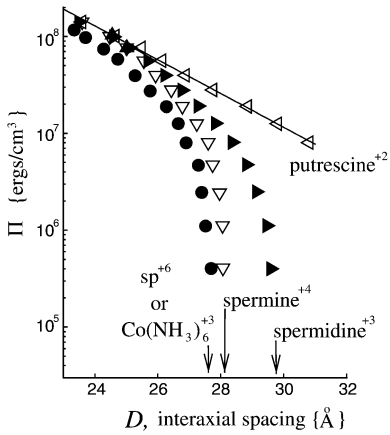


FIGURE 3 Intermolecular pressures between DNA measured by osmotic stress (uncertainties in pressures and interhelical spacings are smaller than symbols). In putrescine (◁), interhelical pressures are purely repulsive and fit a single 2.4 Å decaying exponential (*line*). All of the polyamine measurements (*triangles*) converge to this same curve at high pressures, indicating that the repulsive component of the intermolecular interaction is the same for all. This 2.4 Å exponential is extrapolated to calculate the repulsive component of the free energy for the polyamines. The high-pressure limit is lower for $Co(NH_3)_6Cl_3$ (●), so we use an exponential with correspondingly smaller amplitude. Spermidine (▶), spermine (▽), $sp^{6+}$ (▲; only 3 data points at high and low pressure), and $Co(NH_3)_6Cl_3$ (●) curve down toward a finite separation as $\Pi \rightarrow 0$, indicating spontaneous assembly and attractive forces between helices. Equilibrium interaxial separations, $D_{eq}$, corresponding to $\Pi = 0$, are indicated by arrows.

polynomial form for the attraction and an exponential term for the repulsion (Fig. 1 in the Supplementary Materials, Data S1). We again find that all of the repulsive components of the intermolecular pressure share similar 2.2–2.4 Å characteristic decay lengths. The osmotic stress curves and the fitted decay lengths are insensitive to multivalent cation concentration, consistent with direct spectrophotometric measurements of cation concentrations in the condensed phase (22), modest electrophoretic mobilities of DNA condensates (24), and modeling of DNA-multivalent cation interactions (22,25), all of which suggest that multivalent cation condensed DNA phases maintain a nearly neutralizing amount of bound multivalent cations across a broad range of electrolyte conditions and osmotic pressures.

Comparing the osmotic stress curves for the condensing polyamines (*right solid triangles*, *down open triangles*, *up solid triangles*) with the curve for the +2 charged diamine putrescine (*left open triangle*) that does not condense DNA gives a purely empirical correlate for a 2.2–2.4 Å exponentially decaying repulsion obtained by curve fitting. Inspecting the data at high pressures, each of the condensing polyamine curves appears to converge to the putrescine curve, so that, at the highest experimentally accessible pressure, the interhelical spacings for all of the polyamines are identical to within 0.12 Å. That is, the 2.4 Å single exponential (*line* in Fig. 3), directly observable for putrescine, appears to be the underlying repulsive component for all the polyamines measured. Of course, in the absence of data at higher pressures, we cannot be certain that each of the polyamine curves will continue at this limit indefinitely. However, it is compelling that four different polyamines, starting from four different equilibrium spacings, all reach essentially the same interaxial spacing at the highest measured pressure. It strongly suggests that putrescine represents the pure polyamine repulsion. Moreover, fits of each curve in Fig. 3 to an exponential repulsion and an arbitrary polynomial form for the attraction gave similar decay lengths of 2.2–2.4 Å (Fig. 1 in the Supplementary Material, Data S1) to the 2.4 Å decay length for putrescine. Hence, within the experimental precision, all of the condensing agents exhibit a similar cation-independent 2.2–2.4 Å exponentially decaying repulsion.

We use the 2.4 Å decay length exponential from the putrescine data to describe the repulsive components of the polyamine intermolecular pressures. We use the same curve but with the exponential prefactor reduced by 60% for the repulsive pressure between DNA in $Co(NH_3)_6Cl_3$. Repulsive free energies are calculated by integrating the exponentially repulsive pressures for hexagonally arranged DNA helices (28) to the equilibrium spacing (*arrows* in Fig. 3), $D_{eq}$,

$$\Pi_{rep} = Re^{-D/\lambda_{rep}}, \tag{1}$$

$$\Delta G_{rep} = -\int_{\infty}^{D_{eq}} \Pi_{rep}\sqrt{3}lDdD = \sqrt{3}l\lambda_{rep}(D_{eq}+\lambda_{rep})\Pi_{rep}[D_{eq}], \tag{2}$$

where $\Pi_{rep}$ is the purely repulsive component of the pressure, $R$ is the prefactor to the exponential repulsion, $\lambda_{rep} = 2.4$ Å is the decay length for the repulsive component, and $l = 3.4$ Å is the rise per basepair (Table 1). The uncertainty in $\Delta G_{rep}$ encompasses the range of free energies calculated from the putrescine repulsion and the exponential repulsions obtained by curve fitting.

## Attractive interactions, $\Delta G_{att} = \Delta G - \Delta G_{rep}$

As is apparent in Table 1, the measured free energies of condensation and their repulsive components are similar in magnitude but opposite in sign for each cation. The attractive free energy, $\Delta G_{att}$, equals the difference between the net, $\Delta G$, and repulsion, $\Delta G_{rep}$, and its magnitude is about twice the repulsive free energy. More precisely, the measured values of $-\Delta G_{att}/\Delta G_{rep}$ range from 2.1 to 2.5 and are systematically ~5–25% larger than 2 (Table 1).

The approximate ratio of 2 between attractive and repulsive free energies persists despite qualitative structural and chemical differences between condensing ions and quantitative differences in the stability and interhelical spacing of the condensed DNA. The hexavalent $sp^{6+}$, for instance, is twice the size and has twice the charge of the trivalent spermidine$^{3+}$. The $sp^{6+}$-condensed DNA is 180% more

stable and has an equilibrium interhelical spacing that is 2 Å smaller than spermidine$^{3+}$-condensed DNA (see Table 1). Yet their ratios of $\Delta G_{att}/\Delta G_{rep}$ differ by only 20%. $Co(NH_3)_6Cl_3$, a compact inorganic cation that is chemically and structurally distinct from the polyamines, maintains the same factor $-\Delta G_{att}/\Delta G_{rep} \sim 2$.

## DISCUSSION

Assembly and recognition reactions of biomolecular complexes involve a balance of attractive and repulsive interactions. We combined single-molecule pulling with osmotic-stress ''pushing'' to separate the attractive and repulsive components of the free energy of interaction in DNA condensation. The general strategy should be useful with other complexes, for instance, in determining the interactions that lead to pathogenic protein aggregation.

Although there are nominal configurational differences between coiled-single-molecule condensates and the parallel macroscopic arrays observed under osmotic stress, both are dominated by the intermolecular interactions between helices. On theoretical grounds, single molecule condensates minimize surface and bending effects and, as a result, are expected to assume the same local structure as parallel arrays (29). Hud and Downing confirmed this view experimentally, showing that the helical packing and interhelical spacing in single-molecule $Co(NH_3)_6^{3+}$-DNA condensates (30) closely match those in macroscopic condensed arrays (10). Generally, the total free energy of condensation also includes a loss of DNA configurational entropy. However, the stretched DNA in a magnetic tweezers experiment is already conformationally restricted, so this contribution is negligible. Finally, our direct measurement of the free energy for $Co(NH_3)_6Cl_3$ condensed single molecules, $-0.21\ k_bT$/bp, agrees with a previous estimate, $-0.17\ k_bT$/bp, extrapolated from osmotic stress measurements on macroscopic arrays (10).

Our results reveal two properties of condensed DNA intermolecular interactions that are invariant for all multivalent cations examined. The first is that the repulsive component of the intermolecular pressure decays exponentially with a $2.3 \pm 0.1$ Å characteristic decay length. The second is that the attractive component of the equilibrium free energy is always about twice the repulsive component ($-\Delta G_{att}/\Delta G_{rep} \sim 2.3 \pm 0.2$). These properties hold for all multivalent cations measured, despite differences in their charge, structure, and composition and despite differences in the equilibrium spacing and energetics of the condensed DNA. A third property was consistent for the polyamines, which all share a similar alkyl amine$^+$ monomer but range in length from 2+ to 6+. DNA condensed by polyamines shared, not only the same $2.3 \pm 0.1$ Å repulsive decay length, but also the same magnitude of repulsions (i.e., identical coefficient, $R$ in Eq. 1; see high-pressure limit of Fig. 3). This uniformity is surprising given the strong influence of polyamine length on the condensation free energy (see increasing $\Delta G$ for spermidine$^{3+}$ thru sp$^{6+}$ in Table 1). Uniformity in the repulsive interactions means that differences between DNA condensed by different polyamines are due solely to changes in the attractive component of the intermolecular interaction. Apparently, the attractive component depends very strongly on the length of the polyamine and possibly its arrangement within the condensate, whereas the repulsion does not. These three new empirical constraints should be useful in the development of mechanistic theories for DNA-DNA interactions in the presence of multivalent cations. We present a preliminary evaluation of current theories below.

The condensation of DNA in the presence of counterions might suggest neutralization of electrostatic repulsions and subsequent aggregation by van der Waals forces, as in the Derjaguin-Landau-Verway-Overbeek theory of colloidal flocculation. However, attractions between counterion condensed DNA are at least an order of magnitude larger than expected for van der Waals forces (10). Similarly, ''hydrophobic'' interactions or hydrogen bonding might provide driving forces for aggregation. However, the highly charged DNA surface is clearly not ''hydrophobic'' and the 7–12 Å water-filled space between condensed DNA helices eliminates the possibility of short-range hydrogen bonding. Hence, DNA condensation is commonly attributed to electrostatic attractions.

The predictions of electrostatic theories depend on the approximations used. Mean-field theories, such as the Poisson-Boltzmann equation, that neglect correlations between ions always predict repulsion between like-charged homogeneous surfaces and therefore cannot account for DNA condensation (31). At the other limit, if counterion correlations are very strong, counterions on like-charge apposing surfaces can interlock in a complementary fashion and net attractions result (4,5). Although DNA does not meet the formal criterion for this ''strong coupling'' limit, correlation-induced attractions are apparently still possible (32,33). Detailed Monte Carlo calculations, using parameters described as similar to DNA in $Co(NH_3)_6^{+3}$ or spermidine$^{+3}$, predict attractions that, within 9% error, can be described by an exponential with a decay length equal to the spatial period between neutralizing counterions (33). This decay length is ~2.8 Å for $Co(NH_3)_6^{+3}$ or spermidine$^{+3}$ and increases with the square root of the ion charge for spermine$^{4+}$ and sp$^{6+}$.

We use these decay lengths to compare the predictions of counterion-correlation theory to our experimental results. For exponentially decaying attractive and repulsive intermolecular pressures (e.g., Eq. 2), the ratio of attractive and repulsive free energies at force balance equilibrium ($\Pi_{rep} = \Pi_{att}$) are approximately equal to the ratio of decay lengths,

$$-\frac{\Delta G_{att}}{\Delta G_{rep}} = \frac{\lambda_{att}(D_{eq} + \lambda_{att})}{\lambda_{rep}(D_{eq} + \lambda_{rep})} \cong \frac{\lambda_{att}}{\lambda_{rep}}. \quad (3)$$

Because decay lengths for counterion-correlation repulsions have not been predicted, we use the $\lambda_{rep} = 2.3 \pm 0.1$ Å from our osmotic stress measurements for the repulsive decay

length. Using the predictions of current counterion-correlation theory for $\lambda_{att}$ and the exact form of Eq. 3, we obtain predicted $-\Delta G_{att}/\Delta G_{rep}$ ranging from 1.2 for spermidine or cobalt hexammine to 1.8 for $sp^{6+}$. Differences between the predicted and measured $-\Delta G_{att}/\Delta G_{rep}$ are larger than the uncertainties in our measurements, indicating that the current formulations for counterion-correlation attractions are inconsistent with the experimental data. Perhaps further elaborations of counterion-correlation theory that include additional effects, such as ion excluded-volume (32,34), the spatial patterning of charge on DNA, water structuring, or added electrolyte, can resolve this discrepancy and bring these theories into accord with experiments.

Alternatively, Kornyshev and Leikin have emphasized the role of helical structure in DNA-DNA interactions (6–8). Their formalism shows that the helical structure of DNA can introduce an additional length scale not present when DNA is modeled as a homogeneous rod (7). For the predominant helical period of DNA (34 Å helical pitch divided by $2\pi$), this yields a decay length that is always smaller than 5.4 Å. As with the homogeneous-charged rod, electrostatic attractions cannot result unless counterions are complementary. However, if a line of counterions is assumed bound in the major groove, electrostatic attractions with uniform decay length $<$5.4 Å are possible. Kornyshev and Leikin have also included an image repulsion for the interaction of phosphates and counterions with the low dielectric cores of DNA. This gives a short-range repulsion with a decay length equal to half the decay length for the attraction, or $<$2.7 Å. Using these decay lengths and Eq. 3, Kornyshev's and Leikin's formalism for helical molecules predicts a nearly constant ratio of attractive to repulsive free energy of $-\Delta G_{att}/\Delta G_{rep}\sim 2.2$, consistent with our experimental observations.

We have previously argued that attractions between counterion-condensed DNA are caused by the structuring of water between DNA helices (9,10). The dominating effect that these hydration forces can have on supramolecular organization was first recognized from a common 3.5–4 Å exponentially repulsive force measured between charged, zwitterionic, and uncharged molecules in water (19,35–39). We hypothesized that repulsion resulted from the disruption of structured water between molecules and that the consistent, 3.5–4 Å decay lengths for the measured interactions reflected the ~4 Å correlation length in liquid water (12). Hydration attractions are also theoretically possible if apposing molecular surfaces mutually reinforce the preferred water structure rather than disrupt it. The order-parameter formalism for hydration forces (11) predicts a ~4 Å decay length for attractions and ~2 Å image repulsion due to the steric exclusion of the hydration ''atmosphere'' of one counterion-decorated DNA by an apposing helix (37,40). Using these decay lengths and Eq. 3, the order-parameter formalism for hydration forces predicts a ratio of attractive to repulsive free energy of $-\Delta G_{att}/\Delta G_{rep}\sim 2.1$, consistent with our experimental observations.

The consistency between our experimental results and both hydration forces and electrostatics in Kornyshev's and Leikin's theory of interacting helices is a consequence of the constant ratio of 2 that both theories predict between the decay length for attractive and repulsive interactions ($\lambda_{att}/\lambda_{rep} = 2$). This can easily be seen from Eq. 3, which shows that, for any theory positing exponentially decaying attractive pressures, the ratio of attractive and repulsive free energies at equilibrium is essentially equal to the ratio of the decay lengths. In this case, our two experimental constraints, $\lambda_{rep} = 2.3 \pm 0.1$ Å and $\Delta G_{att}/\Delta G_{rep} = 2.3 \pm 0.2$ indicate a characteristic decay length for condensed DNA attractions of $\lambda_{att} = 4.8 \pm 0.5$ Å. This scheme leads to an equation for the total pressure between helices,

$$\Pi = -Ae^{-D/\lambda} + Re^{-2D/\lambda}, \quad (4)$$

with $\lambda \sim 4.6$ Å and $A$ and $R$ are phenomenological parameters describing the strength of attractions and repulsions, respectively. As an additional critical test of this form, we obtained the coefficient $R$ from osmotic stress measurements, set the coefficient $A$ such that the total pressure is zero at the measured equilibrium spacing, and integrated Eq. 2 to obtain predicted equilibrium free energies. Neither coefficient was fit to the magnetic tweezers data. Predicted (*solid* and *dashed line*) free energies and magnetic tweezers measurements (*symbols*), shown in Fig. 4, closely coincide with a mean discrepancy of 6%, confirming that Eq. 4 accurately describes the intermolecular forces between condensed DNA. In Fig. 4, the homologous series of +3, +4, and +6 polyamines (*triangles*) are seen to fall on a single line. This exponential relationship between the condensation free energy and equilibrium interhelical spacing is predicted only if each ion shares a common underlying repulsion (i.e., the same value for the coefficient $R$ in Eq. 4). This is consistent with our observation that all of the polyamine osmotic stress curves converge to a common limit at high pressure and, likewise, indicates a common repulsion (i.e., the same value $R$).

Although both hydration forces and electrostatics in Kornyshev's and Leikin's theory of interacting helices are consistent with our results, neither theory could be said to predict the measured forces. The order-parameter theory for hydration forces does not include a prediction for the strength of water structuring ($A$ and $R$ in Eq. 4) and hence, does not predict the magnitude of forces. Similarly, the forces predicted by the electrostatic theory of Kornyshev and Leikin depend on the unknown number and location of counterions that are assumed ''bound''. In contrast, counterion-correlation electrostatic theories have made reasonable predictions for the magnitude of DNA-DNA attractions (34,41,42), though the predicted decay lengths appear inconsistent with our measurements. Counterion-correlation electrostatic theories have received a great deal of attention recently because they can rationalize the experimentally observed resolubilization of DNA condensates at high multivalent ion

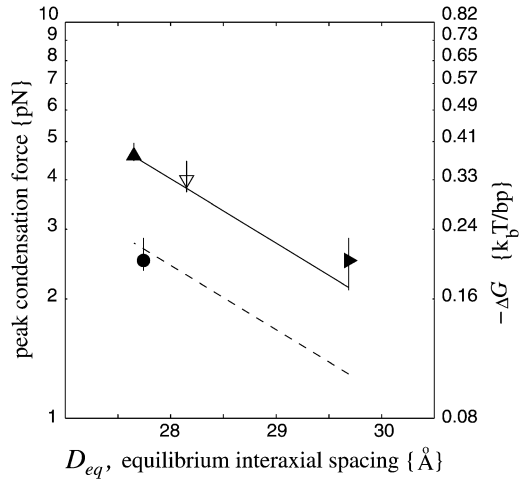


FIGURE 4 Condensation free energy versus equilibrium interaxial separation. The measured condensation free energies for the polyamines, spermidine (▶), spermine (▽), and $sp^{6+}$ (▲) decay exponentially with equilibrium interaxial spacing. $\Delta G$ calculated via Eq. 4, using coefficients $A$ and $R$, determined from osmotic stress experiments, agrees well with the data (*line*). The condensation force for $Co(NH_3)_6Cl_3$ (●) is a factor of 0.52 smaller than would be predicted by the polyamine curve. This is due to the weakened repulsion observed by osmotic stress for $Co(NH_3)_6Cl_3$ as compared to the polyamines (see $D < 26$ Å in Fig. 3). $\Delta G$ calculated via Eq. 4, using a smaller $A$ and $R$, again obtained independently from osmotic stress (*dashed line*), agrees well with the value measured by magnetic tweezers (●). Error bars for the condensation free energies represent the uncertainty in peak determinations from Fig. 2.

concentrations (42) and the observed promotion of DNA condensation in aqueous mixtures of some nonpolar solutes, such as alcohols (43). However, the resolubilization of DNA condensates becomes less mysterious when it is recognized that it occurs near the solubility limit for the multivalent cation salt. The formation of lower-valent anion-associated forms of the multivalent cation that occurs near the solubility limit increases the energetic cost for neutralizing DNA. This increased energetic cost provides a simple mechanism for resolubilization, regardless of the forces that promote DNA condensation (22,26,27). Likewise, electrostatic interpretations of the action of neutral solutes in terms of a change in dielectric constant are only applicable within certain chemically homologous series. The incremental action of alcohols, for instance, orders nicely according to the dielectric constant of the solution (43). Glycerol, on the other hand, has a dielectric constant about half that of water but addition of glycerol to spermidine-DNA solution has no apparent effect on DNA condensation (19,44). The action of neutral solutes correlates more broadly with their extent of exclusion from DNA than with the solution dielectric constant (19), raising doubt that the dielectric constant is causal. In our view, the question of a mechanism for DNA condensation remains open. The new constraints introduced by our measurements should be useful in further development of all of these theories.

## SUPPLEMENTARY MATERIAL

To view all of the supplemental files associated with this article, visit www.biophysj.org.

The authors thank Sergey Leikin and Alexei Kornyshev for useful discussions. B.A.T. thanks Prof. Sanford Leuba for advice on magnetic tweezing of DNA and also gratefully acknowledges support from the labs of Dr. Paul D. Smith (National Institutes of Health/National Institute of Biomedical Imaging and Bioengineering) and Thomas J. Pohida (National Institutes of Health/Center for Information Technology).

Work in the labs of B.A.T., D.C.R., and V.A.P. was supported by the intramural program of the National Institutes of Health/National Institute of Child Health and Human Development. Research in the lab of Dr. Thomas was supported by National Institutes of Health/National Cancer Institute grants CA42439, CA73058, and CA80163.

## REFERENCES

1. Bloomfield, V. A. 1997. DNA condensation by multivalent cations. *Biopolymers*. 44:269–282.
2. Gelbart, W. M., R. F. Bruinsma, P. A. Pincus, and V. A. Parsegian. 2000. DNA-inspired electrostatics. *Phys. Today*. 53:38–44.
3. Ha, B.-Y., and A. J. Liu. 1999. Ha and Liu reply. *Phys. Rev. Lett.* 83:2681.
4. Rouzina, I., and V. A. Bloomfield. 1996. Macroion attraction due to electrostatic correlation between screening counterions. 1. Mobile surface-absorbed ions and diffuse ion cloud. *J. Phys. Chem.* 100: 9977–9989.
5. Shklovskii, B. I. 1999. Wigner crystal model of counterion induced bundle formation of rodlike polyelectrolytes. *Phys. Rev. Lett.* 82:3268–3271.
6. Kornyshev, A. A., D. J. Lee, S. Leikin, and A. Wynveen. 2007. Structure and interactions of biological helices. *Rev. Mod. Phys.* 79:943–996.
7. Kornyshev, A. A., and S. Leikin. 1997. Theory of interaction between helical molecules. *J. Chem. Phys.* 107:3656–3674.
8. Kornyshev, A. A., and S. Leikin. 1999. Electrostatic zipper motif for DNA aggregation. *Phys. Rev. Lett.* 82:4138–4141.
9. Parsegian, V. A., R. P. Rand, and D. C. Rau. 1985. Hydration forces: what next? *Chem. Scr.* 25:28–31.
10. Rau, D. C., and V. A. Parsegian. 1992. Direct measurement of the intermolecular forces between counterion-condensed DNA double helices: Evidence for long range attractive hydration forces. *Biophys. J.* 61:246–259.
11. Marcelja, S., and N. Radic. 1976. Repulsion of interfaces due to boundary water. *Chem. Phys. Lett.* 42:129–130.
12. Xie, Y., K. F. Ludwig, G. Morales, D. E. Hare, and C. M. Sorensen. 1993. Noncritical behavior of density fluctuations in supercooled water. *Phys. Rev. Lett.* 71:2050–2053.
13. Thomas, R. M., T. Thomas, M. Wada, L. H. Sigal, A. Shirahata, and T. J. Thomas. 1999. Facilitation of the cellular uptake of a tripler-forming oligonucleotide by novel polyamine analogues: Structure-activity relationships. *Biochemistry*. 38:13328–13337.
14. Rau, D. C., B. Lee, and V. A. Parsegian. 1984. Measurement of the repulsive force between poly-electrolyte molecules in ionic solution - hydration forces between parallel DNA double helices. *Proc. Natl. Acad. Sci. USA*. 81:2621–2625.
15. Leuba, S. H., M. L. Bennink, and J. Zlatanova. 2004. Methods in Enzymology, Volume 376, Chromatin and Chromatin Remodeling Enzymes, Pt. B. C. David Allis and Carl Wu, editors. Academic Press, San Diego. 73–105.
16. Strick, T. R., J. F. Allemand, D. Bensimon, and V. Croquette. 1998. Behavior of supercoiled DNA. *Biophys. J.* 74:2016–2028.

17. Smith, S. B., L. Finzi, and C. Bustamante. 1992. Direct mechanical measurements of the elasticity of single DNA-molecules by using magnetic beads. *Science*. 258:1122–1126.

18. Parsegian, V. A., R. P. Rand, N. L. Fuller, and D. C. Rau. 1986. Osmotic stress for the direct measurement of intermolecular forces. *Methods Enzymol*. 127:400–416.

19. Hultgren, A., and D. C. Rau. 2004. Exclusion of alcohols from spermidine-DNA assemblies: Probing the physical basis for preferential hydration. *Biochemistry*. 43:8272–8280.

20. Baumann, C. G., V. A. Bloomfield, S. B. Smith, C. Bustamante, M. D. Wang, and S. M. Block. 2000. Stretching of single collapsed DNA molecules. *Biophys. J*. 78:1965–1978.

21. Baumann, C. G., S. B. Smith, V. A. Bloomfield, and C. Bustamante. 1997. Ionic effects on the elasticity of single DNA molecules. *Proc. Natl. Acad. Sci. USA*. 94:6185–6190.

22. Todd, B. A., and D. C. Rau. 2007. Interplay of ion binding and attraction in DNA condensed by multivalent cations. *Nucleic Acids Res*. 10.1093/nar/gkm1038.

23. Murayama, Y., Y. Sakamaki, and M. Sano. 2003. Elastic response of single DNA molecules exhibits a reentrant collapsing transition. *Phys. Rev. Lett*. 90:018102.

24. Besteman, K., K. Van Eijk, and S. Lemay. 2007. Charge inversion accompanies DNA condensation by multivalent cations. *Nature Physics*. 3:641–644.

25. Zhang, R., and B. I. Shklovskii. 2005. The pulling force of a single DNA molecule condensed by spermidine. *Physica A*. 349:563–570.

26. Solis, F. J. 2002. Phase diagram of dilute polyelectrolytes: collapse and redissolution by association of counterions and co-ions. *J. Chem. Phys*. 117:9009–9015.

27. Yang, J., and D. C. Rau. 2005. Incomplete ion dissociation underlies the weakened attraction between DNA helices at high spermidine concentrations. *Biophys. J*. 89:1932–1940.

28. Podgornik, R., H. H. Strey, K. Gawrisch, D. C. Rau, A. Rupprecht, and V. A. Parsegian. 1996. Bond orientational order, molecular motion, and free energy of high-density DNA mesophases. *Proc. Natl. Acad. Sci. USA*. 93:4261–4266.

29. Tzlil, S., J. T. Kindt, W. M. Gelbart, and A. Ben-Shaul. 2003. Forces and pressures in DNA packaging and release from viral capsids. *Biophys. J*. 84:1616–1627.

30. Hud, N. V., and K. H. Downing. 2001. Cryoelectron microscopy of lambda phage DNA condensates in vitreous ice: The fine structure of DNA toroids. *Proc. Natl. Acad. Sci. USA*. 98:14925–14930.

31. Neu, J. C. 1999. Wall-mediated forces between like-charged bodies in an electrolyte. *Phys. Rev. Lett*. 82:1072–1074.

32. Deserno, M., A. Arnold, and C. Holm. 2003. Attraction and ionic correlations between charged stiff polyelectrolytes. *Macromolecules*. 36:249–259.

33. Naji, A., S. Jungblut, A. G. Moreira, and R. R. Netz. 2005. Electrostatic interactions in strongly coupled soft matter. *Physica A*. 352:131–170.

34. Tan, Z., and S. Chen. 2006. Ion-mediated nucleic acid helix-helix interactions. *Biophys. J*. 91:518–536.

35. Bonnet-Gonnet, C., S. Leikin, S. Chi, D. C. Rau, and V. A. Parsegian. 2001. Measurement of forces between hydroxypropylcellulose polymer: Temperature favored assembly and salt exclusion. *J. Phys. Chem. B*. 105:1877–1886.

36. Chik, J., S. Mizrahi, S. Chi, V. A. Parsegian, and D. C. Rau. 2005. Hydration forces underlie the exclusion of salts and of neutral polar solutes from hyroxypropylcellulose. *J. Phys. Chem. B*. 109:9111–9118.

37. Leikin, S., V. A. Parsegian, D. C. Rau, and R. P. Rand. 1993. Hydration forces. *Annu. Rev. Phys. Chem*. 44:369–395.

38. McIntosh, T. J. 2000. Short-range interactions between lipid bilayers measured by X-ray diffraction. *Curr. Opin. Struct. Biol*. 10:481–485.

39. Strey, H. H., R. Podgornik, D. C. Rau, and V. A. Parsegian. 1998. DNA-DNA interactions. *Curr. Opin. Struct. Biol*. 8:309–313.

40. Kornyshev, A. A., and S. Leikin. 1989. Fluctuation theory of hydration forces: The dramatic effects of inhomogenous boundary conditions. *Phys. Rev. A*. 40:6431–6437.

41. Raspaud, E., D. Durand, and F. Livolant. 2005. Interhelical spacing in liquid crystalline spermine and spermidine-DNA precipitates. *Biophys. J*. 88:392–403.

42. Nguyen, T. T., I. Rouzina, and B. I. Shklovskii. 2000. Reentrant condensation of DNA induced by multivalent counterions. *J. Chem. Phys*. 112:2562–2568.

43. Arscott, P. G., C. Ma, J. R. Wenner, and V. A. Bloomfield. 1995. DNA condensation by cobalt hexammine (III) in alcohol-water mixtures: Dielectric constant and other solvent effects. *Biopolymers*. 36:345–364.

44. Stanley, C., and D. C. Rau. 2006. Preferential hydration of DNA: The magnitude and distance dependence of alcohol and polyol interactions. *Biophys. J*. 91:912–920.